ACS APPLIED ENERGY MATERIALS

www.acsaem.org

Article

W-Doped $BiVO_4$ Photoanodes for Light-to-Chemical Energy Conversion

Milda Petruleviciene, Kaja Spilarewicz, Irena Savickaja, Jurga Juodkazyte, Joanna Kuncewicz, Grażyna Stochel, Wojciech Macyk, and Arunas Ramanavicius*

Cite This: *ACS Appl. Energy Mater.* 2025, 8, 7919−7928

Read Online

ACCESS | Metrics & More | Article Recommendations | Supporting Information

ABSTRACT: Renewable energy and related systems are an indispensable part of our future. The urgent need to tackle climate change and the energy crisis has driven the search for innovative alternative technologies to replace current polluting and energy-intensive ones. Photoelectrochemical (PEC) advanced oxidation systems offer the possibility to convert light energy into chemical energy and store it in the form of valuable chemical compounds, e.g., oxidants and hydrogen. In this study, the performance of sol−gel-derived W-doped $BiVO_4$ in photoelectrolysis of aqueous sulfate solutions was investigated. W-doping was found to have a significant impact on the PEC activity of the material, with optimal results achieved using 1−5 atom % of the dopant. Fluorescence lifetime imaging microscopy revealed variations in material quality, which were attributed to the defects in the $BiVO_4$ crystal lattice introduced by W-doping. The double maxima observed in the incident photon-to-current efficiency maps and applied-bias photon-to-current efficiency plots were explained by the dopant-related introduction of electronic states, which require lower energy input for their excitation and participation in the interfacial charge transfer reactions. Analysis of the charge separation efficiencies in the bulk and on the surface of the layers revealed that separation in the bulk is the limiting factor for all the studied materials, whereas W-doping reduces the charge carrier recombination at the photoelectrode surface. The latter effect was ascribed to the superficial position of $BiVO_4$ lattice defects introduced by W-doping. Light-driven generation of persulfate and hydrogen was demonstrated.

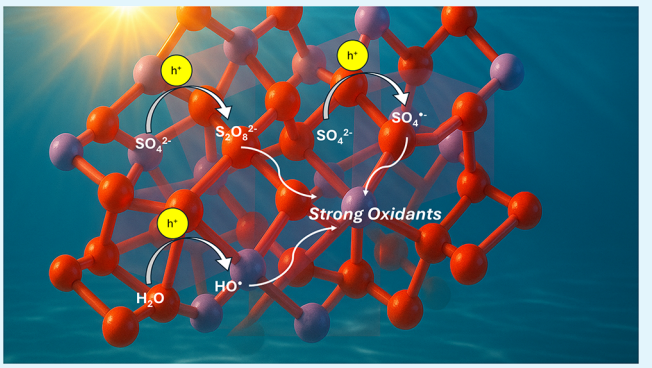

KEYWORDS: *bismuth vanadate, W-doping, photoelectrochemical energy conversion, hydrogen, persulfate*

1. INTRODUCTION

Renewable energy sources are essential for achieving energy independence from natural gas, oil and fossil fuels. They also play a key role in combating climate change. The production of green hydrogen through water electrolysis using renewable (wind and solar) electricity is regarded as a pivotal step in the transition to a more sustainable future.[1,2] PEC advanced oxidation systems (PEC AOSs) offer another method to harness solar energy. They can be used to produce valuable chemicals (such as hydrogen, oxidants organic compounds) or for applications like pollutant removal, wastewater treatment, and disinfection.[2−6] The efficiency of these processes is strongly dependent on the nature of semiconductor photoelectrode as well as electrolyte.[7−11] Notable examples of photoanodes include ZnO, WO_3, $BiVO_4$, TiO_2, and Fe_2O_3.[12−15] $BiVO_4$ is a widely investigated semiconductor material for PEC watersplitting and other photocatalytic applications. Its band gap of 2.4−2.5 eV allows effective absorption of visible light[16] and its stability in neutral aqueous environment makes it an ideal candidate for solar energy conversion.[17] However, one of the main challenges associated with the use of $BiVO_4$ is its relatively short charge carrier diffusion length, resulting in a high recombination rate of photoexcited electrons and holes. Therefore, researchers are exploring methods to increase the diffusion length as well as to enhance the moderate charge carrier mobility of the material. This is important because it affects the material's efficiency in transporting charges to the surface for catalytic reactions.[18,19] These challenges can be mitigated by modifying $BiVO_4$ with elements like Cr, Zr, Zn, Li, Mo and W.[18,20,21] However, careful optimization of the doping level and composition is essential to avoid creating excess defect sites, such as Bi, V, and O vacancies, which may serve as recombination centers.[16] According to a recent DFT study,[22] Fermi levels in W/Mo-doped monoclinic $BiVO_4$ vary under different growth

Received: January 19, 2025
Revised: May 8, 2025
Accepted: May 13, 2025
Published: June 5, 2025

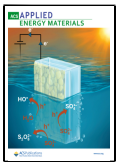

conditions due to defect creation. The formation energies of vacancy defects, including Bi vacancy (Vac_{Bi}), V vacancy (Vac_V) and O vacancy (Vac_O), in W/Mo-doped monoclinic $BiVO_4$ are different. While W atoms substitute for V atoms regardless of growth conditions, unintentional compensation of native point defects, particularly Vac_{Bi}, which has low defect formation energy, results in distinct physical properties.[23] The easier ionization of the W_V defect leads to increased oxidation reactions at the surface and superior photocatalytic activity compared to undoped $BiVO_4$.[22] Zhao et al., on the basis of theoretical and experimental analysis, suggested that the introduction of W-doping changes the active sites and adsorption of water and oxygen evolution reaction intermediates (OH_{ads}, O_{ads}, and OOH_{ads}) on the surface of $BiVO_4$, thus greatly enhancing the surface charge transfer and PEC watersplitting performance.[24] However, depending on the composition of the electrolyte, other oxidation reactions may occur on the surface of the $BiVO_4$ photoanode. For example, in chloride or sulfate electrolytes, the formation of ClO^- or $S_2O_8^{2-}$, respectively, has been reported.[10,25−27] This suggests the possibility of adsorption of other reacting species, as well.

This study examines the impact of tungsten doping on the PEC activity of $BiVO_4$ coatings in Na_2SO_4 electrolyte. During the sol−gel synthesis process, tungsten was introduced in varying concentrations (1, 5, and 10 atom % of tungsten) to progressively increase W-doping and synthesize $BiV_{1-x}W_xO_4$, with the aim of enhancing charge carrier density through W substitution at V sites. The coatings were characterized using the methods of X-ray diffraction (XRD), scanning electron microscopy (SEM), energy-dispersive X-ray (EDX), incident photon-to-current efficiency (IPCE), diffuse reflectance spectroscopy (DRS), surface photovoltage (SPV), fluorescence-lifetime imaging microscopy (FLIM), electrochemical impedance spectroscopy (EIS), linear sweep voltammetry (LSV), and chronoamperometry (CA). The results showed a notable enhancement in PEC activity with the incorporation of tungsten. The optimal results were achieved with 1 and 5 atom % of W. Light-induced production of reactive sulfate species and hydrogen in the PEC cell with W-doped $BiVO_4$ photoanode was demonstrated. Analysis of the factors that limit the performance of the W-doped $BiVO_4$ films is presented. W-doping is shown to facilitate charge separation at the photoelectrode surface.

2. MATERIALS AND METHODS

2.1. Materials. Bismuth(III) nitrate pentahydrate ($Bi(NO_3)_3 \cdot 5H_2O$) from Carl Roth (Karlsruhe, Germany), ammonium vanadate (NH_4VO_3) from Acros Organics (Kandel, Germany), nitric acid (HNO_3) from Reachmen (Bratislava, Slovakia), sodium sulfate (Na_2SO_4) from Acros Organics (Kandel, Germany), as well as sodium tungstate (Na_2WO_4) from Carl Roth (Karlsruhe, Germany), citric acid ($C_6H_8O_6$) from Carl Roth (Karlsruhe, Germany), poly(vinyl alcohol) (PVA) from Acros Organics (Kandel, Germany) and acetic acid (CH_3COOH) from Reachmen (Bratislava, Slovakia) were used as received from suppliers without further purification.

2.2. Synthesis of $BiVO_4$ and W-Doped $BiVO_4$ Coatings. The sol−gel method was used to produce $BiVO_4$ coatings. A mixture of 2.94 g of $Bi(NO_3)_3 \cdot 5H_2O$ and 0.702 g of NH_4VO_3 (molar ratio of 1:1) was dissolved in 23% HNO_3. Subsequently, 2.52 g of $C_6H_8O_7$ was added to the solution under continuous stirring, resulting in the formation of a transparent blue solution. The sol viscosity was adjusted by incorporating 1 g of PVA and 3 mL of acetic acid and the solution was maintained at 50 °C for 24 h with the aid of a magnetic stirrer.

The synthesis of W-doped $BiVO_4$ (with 1, 5 and 10 atom % of W) was achieved by dissolving calculated amounts of Na_2WO_4 in 15 mL of distilled water and adding it to the aforementioned $BiVO_4$ solution after 4 h of mixing. The mixtures were subsequently stirred overnight (12 h) on a magnetic stirrer at 20 °C. The resulting sol−gel was then used to deposit thin films on fluorine-doped tin oxide (FTO) substrates (2.5 × 2.5 cm^2), which were thoroughly precleaned under ultrasonication in acetone, isopropanol and water for 15 min in each.

The dip-coating procedure was performed using a dip-coater (Nadetech, ND-DC 11/1) at a rate of 100 mm/min for both immersion and withdrawal, with a duration of 60 s. The layers were annealed at 450 °C in air (1 °C/min) to achieve crystalline $BiVO_4$ and W-doped $BiVO_4$ coatings. The deposition process was repeated twice. The samples employed in this study are designated as follows: $BiVO_4$, W1_$BiVO_4$, W5_$BiVO_4$, and W10_$BiVO_4$. The numerals 1, 5, and 10 indicate the atomic percentage of tungsten used in the synthesis.

2.3. Structural, morphological, spectroscopic, and optical analysis of $BiVO_4$ and W-doped $BiVO_4$ coatings. The crystalline structure of synthesized $BiVO_4$ coatings was investigated using an X-ray diffractometer SmartLab (Rigaku) equipped with a 9 kW rotating Cu anode X-ray tube. The analysis covered a 2θ range of 20−80°, utilizing the grazing incidence GIXRD method with a 0.5° angle (ω) set between a parallel beam of X-rays and the specimen surface. Phase identification was conducted using Match software in conjunction with the Crystallography Open Database (COD).

The surface morphology of prepared samples was analyzed by SEM imaging using a Helios NanoLab dual beam and Helios 5 Hydra DualBeam (Thermo Scientific) in immersion mode. Mapping and element analysis were carried out with a Helios NanoLab dual-beam workstation (Oxford Instruments, Netherlands) equipped with an EDX spectrometer from Oxford Instruments using 10 and 20 kV.

The DRS measurements were performed with a Shimadzu UV-3600 UV−Vis-NIR spectrophotometer equipped with a 10 cm diameter integrating sphere, and pure $BaSO_4$ was used as a reference. Bandgap energies (E_g) of the films were determined by extrapolating the linear region of the $(F(R)h\nu)^{1/2}$ vs $h\nu$ plots, where $F(R)$ is Kubelka−Munk transformation function, h is Planck's constant, ν is the frequency of the photon, and 1/2 is the Tauc exponent for direct transitions.

FLIM measurements were carried out using a confocal MicroTime 200 system (PicoQuant, GmbH) coupled to an OLYMPUS IX83 microscope equipped with a 60× water-immersed objective (NA 1.2, OLYMPUS UPlanAPO). The samples were excited with a pulsed 370 nm laser.

2.4. PEC Investigations. LSV, open-circuit potential (OCP) and EIS measurements were performed in the three-electrode electrochemical cell using potentiostat/galvanostat Zennium/Zahner Xpot (Zahner Elektrik, Germany) in 0.5 M Na_2SO_4 (Acros Organics, Kandel, Germany). $BiVO_4$ coatings deposited on FTO substrates were used as the working electrodes. Silver/silver chloride electrode with saturated KCl solution ($Ag/AgCl_{(sat.\ KCl)}$) and Pt plate (1 × 1 cm^2) were used as reference and counter electrodes, respectively. All potential values in the paper were reported vs $Ag/AgCl_{(sat.\ KCl)}$ unless noted otherwise. The surface of working electrodes was illuminated with a LED solar simulator (Redoxme, Sweden) providing natural sunlight (AM1.5G) in the wavelength range of 350 to 1050 nm with a power density of 100 mW cm^{-2}. The Nyquist plots were measured at 0.7 V with an AC amplitude of 10 mV, within the frequency range of 10^4 to 0.1 Hz under illumination.

Mott−Schottky measurements were conducted in the dark at a constant frequency of 1000 Hz in 0.5 M Na_2SO_4 electrolyte, using an AC voltage amplitude of ±10 mV. The donor density (N_D) was determined from the slope of the $1/C^2$ versus E plot, based on the following equation:[35]

$$\frac{1}{C^2} = \frac{2}{\varepsilon\varepsilon^0 A^2 e N_D}\left(E - E_{FB} - \frac{K_B T}{e}\right) \quad (1)$$

https://doi.org/10.1021/acsaem.5c00150
ACS Appl. Energy Mater. 2025, 8, 7919−7928

where C represents the specific capacitance (F cm^{-2}), ε is the relative permittivity of the semiconductor (86 for $BiVO_4$[45]), and ε^0 is the permittivity of vacuum (8.854×10^{-14} F cm^{-1}). A denotes the electrode area (cm^2), e is the elementary charge (1.60×10^{-19} C), N_D is the donor density (cm^{-3}), E is the applied electrode potential, E_{FB} is the flat band potential, K_B is the Boltzmann constant and T is the absolute temperature.

SPV was studied using an environmental Kelvin probe (Instytut Fotonowy, Poland) retrofitted with a xenon lamp (150 W) and a monochromator. The contact potential difference (CPD) of the sample irradiated with intermittent light (in the range of 280−500 nm) was measured using the Au 2.5 mm diameter mesh.

IPCE was studied in a three-electrode single-compartment cell with a potentiostat (Instytut Fotonowy, Poland) equipped with a xenon lamp (150 W) and a monochromator. IPCE of the working electrode with the studied material was measured under irradiation of 300−600 nm. The counter electrode used was Pt wire, and the reference electrode was Ag/AgCl.

Applied-bias photon-to-current efficiency (ABPE, %) measurements were performed in a two-electrode cell using $BiVO_4$ and W-doped $BiVO_4$ coatings and a Pt plate as photoanodes and cathode, respectively. Measurements were performed at a 50 mV s^{-1} scan rate within 0−2.5 V applied bias range in 0.1 M Na_2SO_4 electrolyte. ABPE (%) was calculated using the equation:

$$\mathrm{ABPE}(\%) = \frac{I_{ph}(|E^0| - E_{bias})}{P_{sun}} \times 100\% \quad (2)$$

where I_{ph} is photocurrent density (mA cm^{-2}), E^0 is the thermodynamic potential of a reaction (V), E_{bias} is applied bias (V) and P_{sun} is illumination power density (100 mW cm^{-2}). E^0 was evaluated presuming that the photoanodic reaction in Na_2SO_4 electrolyte is

$$2SO_4^{2-} \rightarrow S_2O_8^{2-} + 2e^- \quad E^0_{anode} = 2.01\ \mathrm{V(SHE)} \quad (3)$$

whereas the cathodic process occurring on the Pt electrode is a hydrogen evolution reaction

$$2H^+ + 2e^- \rightarrow H_2$$

$$E^0_{cathode} = 0 - 0.059\ \mathrm{pH} = -0.413\ \mathrm{V(SHE)}\ \text{at pH 7} \quad (4)$$

Consequently, the theoretic potential of cell reaction, $E^0 = E^0_{cathode} - E^0_{anode} = -0.413 - 2.01 = -2.423$ V, where the minus sign indicates that the process is nonspontaneous.

The performance of a photoelectrode was analyzed by calculating the charge separation yield in the bulk material and on the surface.[30,46] The total photocurrent in the absence of a hole scavenger can be described by eq 5:

$$J^{H_2O} = J_{abs} \times \eta_{bulk} \times \eta_{surf} \quad (5)$$

in which J_{abs} is the photon absorption rate expressed as a current, η_{bulk} is the charge separation yield in the bulk, and η_{surf} is the charge separation yield at the surface. When sodium sulfite (Na_2SO_3) is added to the electrolyte, it acts as a highly effective hole scavenger. This results in a 100% surface charge separation yield ($\eta_{surf} = 1$), resulting in eq 6:

$$J^{SO3} = J_{abs} \times \eta_{bulk} \quad (6)$$

Based on eqs. 5 and 6, the charge separation yields in the bulk and on the surface can be obtained:

$$\eta_{bulk} = J^{SO3}/J_{abs} \quad (7)$$

$$\eta_{surf} = J^{H_2O}/J^{SO3} \quad (8)$$

J^{SO3} and J^{H2O} are photocurrents measured in electrolytes with and without sulfite as a hole scavenger, respectively. In calculations, J_{abs} = 7.5 mA cm^{-2} was used as the theoretical maximum available photocurrent of $BiVO_4$.[30]

Reactive sulfate species (RSSs) were generated by conducting photoelectrolysis in a 0.1 M Na_2SO_4 electrolyte using a two-electrode cell. An applied bias of 1.2 V (vs Pt cathode) was used until a charge of approximately 0.5 C had passed through the system. When using a $BiVO_4$ photoanode, only 0.02 C of charge was passed due to the negligible photocurrent. The electrolyte from the anodic compartment of the cell was then collected and analyzed for the presence of RSS in the form of $S_2O_8^{2-}$ using chromatometric titration as described in our previous works.[8,40] The theoretic amount of RSS, denoted as m_{theor}, was calculated using Faraday's law taking into account the electric charge, Q (in C), passed through the cell during photoelectrolysis and assuming the two-electron transfer in the oxidation of SO_4^{2-} to $S_2O_8^{2-}$ (eq 3). The Faradaic efficiency (FE, %) for the PEC generation of RSS was determined by evaluating the ratio $m_{exp}/m_{theor} \times 100$.

H_2 evolution on Pt cathode was studied using the hydrogen microsensor (H_2-NPLR) and UniAmp amplifier (Unisense, Denmark) in the two-electrode cell under illumination and applied bias of 1.2 V (vs Pt). The microsensor's tip was immersed in the cathodic compartment of the cell near the surface of Pt electrode.

Photocurrent stability tests were performed in 0.1 M Na_2SO_4 under applied bias of 1.2 V (vs Pt).

3. RESULTS AND DISCUSSION

3.1. Structural, Morphological, Electronic, and Optical Properties of W-Modified $BiVO_4$ Coatings. The materials with different tungsten contents (0, 1, 5, and 10 atom %), abbreviated as $BiVO_4$, W1_$BiVO_4$, W5_$BiVO_4$, and W10_$BiVO_4$, were synthesized with the sol−gel method using a dip-coating deposition on the FTO substrate. Peaks in diffractograms (Figure 1) were assigned to monoclinic $BiVO_4$ (COD: 9013436) and SnO_2 (COD: 9009082) from FTO. The diffractograms look almost the same for all coatings, and no clear shift of peaks is observed, indicating similar lattice parameters for all samples. A minor difference is that the peak at $2\theta = 35°$ is single in W-doped samples, while two peaks are present in undoped $BiVO_4$. This observation is consistent with the XRD data reported in ref 28 and could be considered as an indication of W incorporation into the crystal lattice of $BiVO_4$. Successful incorporation of W into $BiVO_4$ layers was evidenced through EDX elemental mapping analysis, where the signal of W increased consistently with the amount of W used in the synthesis and corresponded to 0.14, 0.55, and 0.87% of W for W1_$BiVO_4$, W5_$BiVO_4$, and W10_$BiVO_4$ coatings, respec-

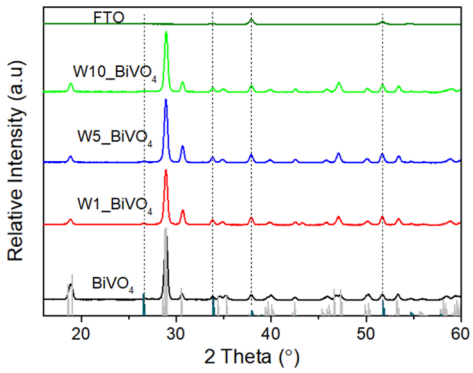

Figure 1. X-ray diffractograms of $BiVO_4$, W1_$BiVO_4$, W5_$BiVO_4$, and W10_$BiVO_4$ coatings and bare FTO substrate. Gray columns represent the reference pattern for $BiVO_4$ (COD: 9013436) and green columns correspond to the reference pattern for SnO_2 (COD: 9009082).

https://doi.org/10.1021/acsaem.5c00150
ACS Appl. Energy Mater. 2025, 8, 7919−7928

tively (Table 1). The EDX analysis also shows a uniform distribution of elements in the samples (Figure S1).

Table 1. Elemental Composition of the Synthesized Coatings

Sample	O, atom %	V, atom %	W, atom %	Bi, atom %
$BiVO_4$	72.03	13.68	-	14.26
W1_$BiVO_4$	81.05	9.70	0.14	9.11
W5_$BiVO_4$	81.00	9.23	0.55	9.21
W10_$BiVO_4$	80.69	9.07	0.87	9.30

The SEM analysis was performed to evaluate the morphology of the synthesized coatings. The $BiVO_4$ coatings appear to consist of a network of round and elongated particles, typical of monoclinic bismuth vanadate produced through the sol−gel process.[29] All films have a porous structure, although the particles vary in size, shape and degree of coalescence depending on the dopant concentration (Figure 2). The thickness of $BiVO_4$ coatings is 50−80 nm (Figure S2).

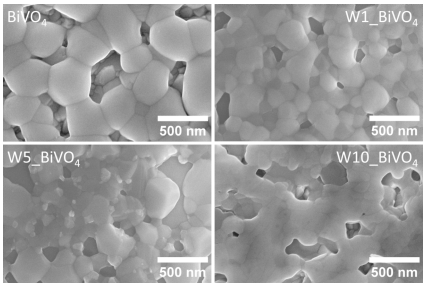

Figure 2. SEM images of $BiVO_4$, W1_$BiVO_4$, W5_$BiVO_4$, and W10_$BiVO_4$ coatings.

SPV measurements were conducted to assess the influence of W-doping on the photoresponse of the materials within the 280−500 nm range (Figure 3 and Figure S3). Since $BiVO_4$ is

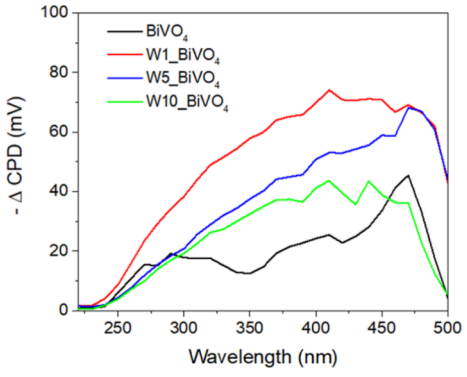

Figure 3. SPV spectra of the $BiVO_4$, W1_$BiVO_4$, W5_$BiVO_4$, and W10_$BiVO_4$ coatings.

an *n*-type semiconductor, the positive values of the ΔCPD are expected. However, due to the low thickness of the coating and the contact with FTO, the observed ΔCPD is negative, which can be explained by hole transfer from $BiVO_4$ to FTO[30] and multiple trapping model observed for mesoporous $BiVO_4$.[31] For the unmodified $BiVO_4$, the highest |ΔCPD|, which reflects the most efficient charge separation, is observed at 470 nm. However, the photoresponse decreases by up to ∼55% for lower wavelengths in the visible spectral range and even more for incident UV light. Such a decrease is not visible for W1_$BiVO_4$, the photoresponse of which is uniform in the 400−470 nm light range, with a significant improvement in the ability of visible light harvesting. Moreover, this coating exhibits the highest values of |ΔCPD| and therefore the most efficient charge separation compared to other studied materials. The W5_$BiVO_4$ achieves a similar photoresponse with maximum at 470 nm and then exhibits the same decrease as unmodified material. As the amount of dopant is increased, the efficiency of the charge separation is further reduced (Figure 3).

More significant charge recombination in the unmodified $BiVO_4$ and W10_$BiVO_4$ materials compared to other samples has been manifested by the fluorescence-lifetime imaging microscopy experiments. The FLIM images of $BiVO_4$ and W10_$BiVO_4$ in Figure 4 show numerous bright spots

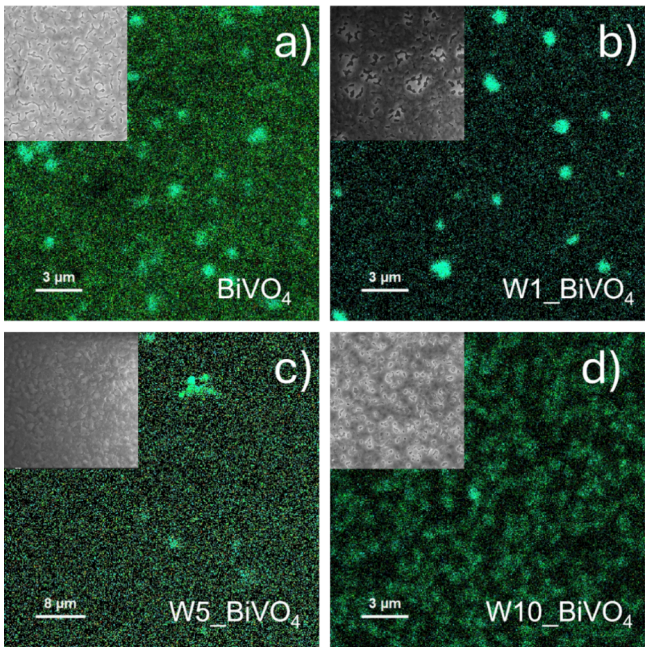

Figure 4. FLIM images registered for (a) $BiVO_4$, (b) W1_$BiVO_4$, (c) W5_$BiVO_4$ and (d) W10_$BiVO_4$ samples with inserted SEM images of the coatings. The images in each pair are on the same scale.

associated with a high luminescence intensity. A much lower density of these spots is observed for the W1_$BiVO_4$ sample, while images of the W5_$BiVO_4$ material contain only a limited number of such areas. Moreover, luminescence decay rates determined for samples containing 1 and 5% W dopant are higher than those for bare $BiVO_4$. In general, efficient luminescence may indicate significant photoinduced charge carrier recombination, which is not desirable in PEC processes. The studied materials in FLIM experiments have been immersed in water; thus, efficient luminescence suggests poor charge transfer between the photoelectrodes and solvent. Poor charge transfer could be related to locally deteriorated charge carriers' separation, which could be caused by a poorer connection of the material with the surrounding. Such places in which locally inefficient charge flow between the material and FTO substrate causes charging of the materials are clearly visible in the SEM images acquired in immersion mode (insets in Figure 4). The arrangement and density of such distinct

https://doi.org/10.1021/acsaem.5c00150
ACS Appl. Energy Mater. 2025, 8, 7919−7928

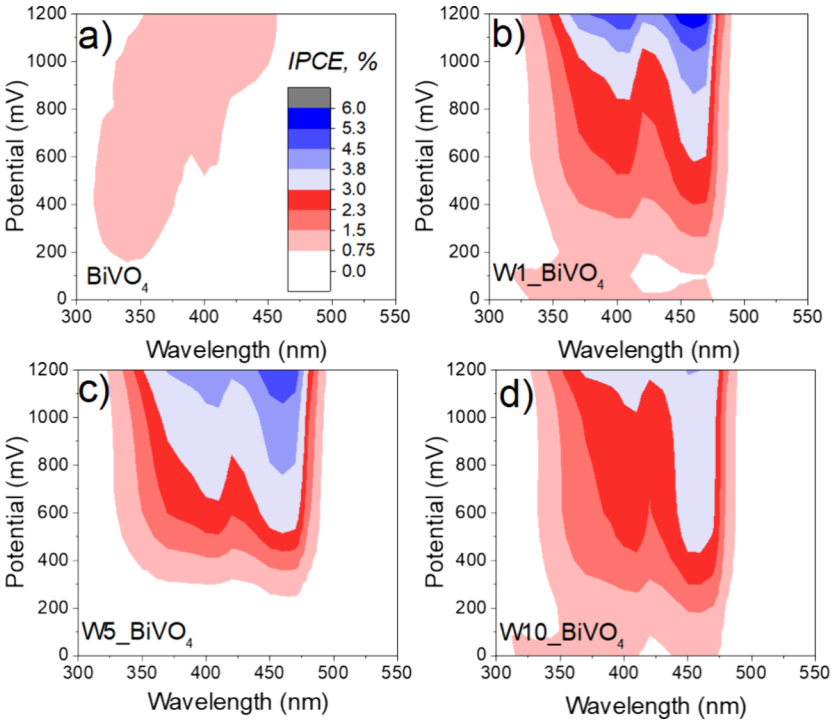

Figure 5. IPCE maps for $BiVO_4$ (a), W1_$BiVO_4$ (b), W5_$BiVO_4$ (c), and W10_$BiVO_4$ (d) coatings measured in 0.5 M Na_2SO_4 electrolytes.

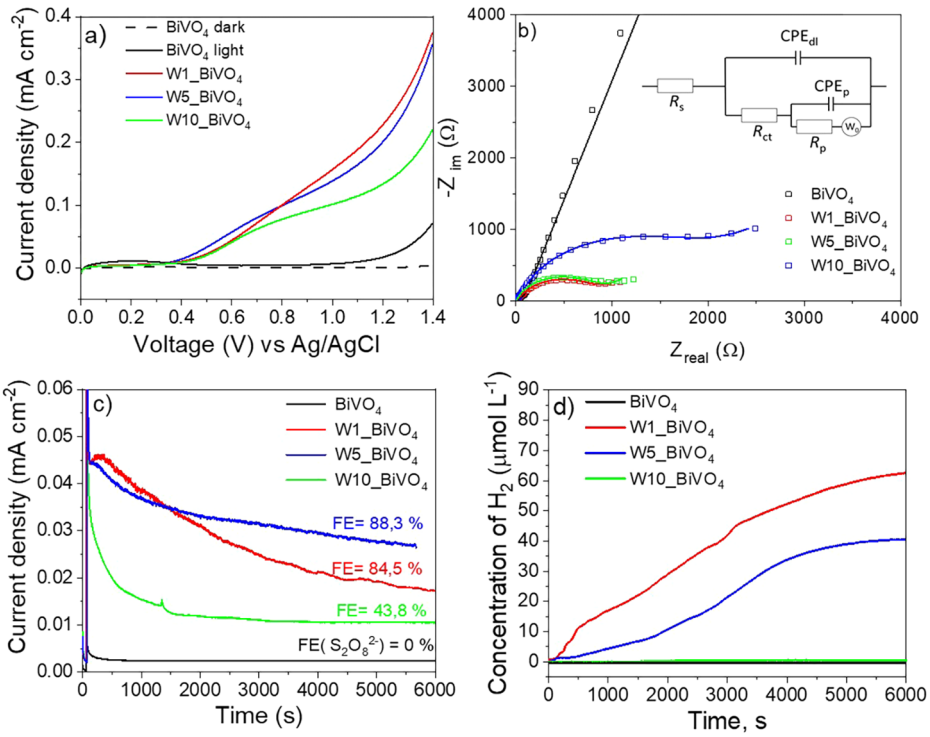

Figure 6. (a) LSVs of $BiVO_4$, W1_$BiVO_4$, W5_$BiVO_4$, and W10_$BiVO_4$ coatings in 0.5 M Na_2SO_4, 50 mV s^{-1}, power of illumination 100 mW cm^{-2}; (b) Nyquist plots recorded at 0.7 V with 10 mV amplitude under illumination in 0.5 Na_2SO_4; (c) variation of photocurrent and (d) concentration of hydrogen during photoelectrolysis at 1.2 V (vs Pt) in 0.1 M Na_2SO_4 using indicated coatings as photoanodes; values of Faradaic efficiency of light-induced generation of persulfate are indicated at corresponding chronoamperograms in panel (c) (limits of experimental error ± 5%).

bright spots prove locally poorer electron drainage, corresponding to bright spots in FLIM images. A worse connection between the material and the substrate may stem from insufficient adhesion or indirect contact of film fragments to the substrate. More efficient recombination could also be related to efficient trapping of the charges in deeper traps, causing a drop in the electrochemical potential of the photogenerated charges.

https://doi.org/10.1021/acsaem.5c00150
ACS Appl. Energy Mater. 2025, 8, 7919−7928

Table 2. Values of Resistance from the EIS Fitted Model and Charge Carrier Density (N_D) of $BiVO_4$, W1_$BiVO_4$, W5_$BiVO_4$, and W10_$BiVO_4$ Coatings

Sample	R_s, Ω	R_{ct}, Ω	CPE_{dl}, μS	R_p, Ω	CPE_p, μS	error (%)	N_D (slope 1), cm^{-3}	N_D (slope 2), cm^{-3}
$BiVO_4$	6.48	149	41.5	114M	89	3.54	5.10×10^{18}	-
W1_$BiVO_4$	7.79	71.4	16.4	803	134	1.7	1.06×10^{19}	1.59×10^{19}
W5_$BiVO_4$	7.41	29.7	8.05	874	92.5	2.45	1.21×10^{19}	3.59×10^{19}
W10_$BiVO_4$	7.92	140	23.0	1800	61.2	1.04	5.62×10^{19}	4.93×10^{19}

3.2. PEC Performance of W-Modified $BiVO_4$ Coatings.

The synthesized coatings were further subjected to photocurrent spectroscopy measurements in 0.5 M Na_2SO_4. The 2D mapping graphs in Figure 5 reveal the variation of IPCE as a function of the wavelength and electrode potential. The results demonstrate that W-doping enhances the PEC activity of $BiVO_4$. The edge of IPCE increase for W-doped $BiVO_4$ coatings is observed at ∼490 nm, which is consistent with the band gap (E_g) values of ∼2.5 eV found from DRS measurements (Figure S4a). Obtained E_g values correlate well with literature data.[32,33] The IPCE values of the W1_$BiVO_4$ and W5_$BiVO_4$ coatings were the highest, reaching approximately 5−6% in the potential range of 1.1−1.2 V at a wavelength of 470 nm, which is coherent with the results of SPV measurements (Figure 3). However, the IPCE of the W10_$BiVO_4$ coating was almost half that of the best-performing coatings. It should be noted that W-doping does not affect the spectral range of the photoresponse, only its efficiency. Furthermore, it can be observed that in the case of W-doped coatings, IPCE has two peaks at ∼400 and ∼470 nm (Figure 5b−d), whereas this phenomenon is not observed for the undoped layer (Figure 5a). It is interesting to note that the peak at longer wavelengths starts to increase at lower potentials. This suggests that a fraction of charge carriers requires lower energy input (light and electrical) to reach the surface and engage in interfacial charge transfer reactions. The presence of two peaks in IPCE spectra is consistent with the inhomogeneity of bright spots observed in FLIM spectra (Figure 4), implying the variability of the PEC activity of the synthesized materials. It is known from the literature that IPCE values and their peak positions can vary depending on the synthesis conditions, dopant and applied bias.[34−37] IPCE values of 5.79,[38] 8,[35] and 9−12%[39] have been reported for W-doped $BiVO_4$ coatings, with improved kinetics of photooxidation reactions compared to undoped $BiVO_4$ (IPCE ∼2%).

In the next step, the PEC performance of the coatings was characterized under white light illumination of a LED solar simulator with 100 mW cm^{-2} intensity. Variation of the OCP of studied $BiVO_4$ photoelectrodes in response to chopped illumination is shown in Figure S5. A negative shift in the OCP under illumination is characteristic of n-type semiconductors, however, the transient behavior differs significantly between W-doped and undoped samples. The absence of transient spikes and the rapid stabilization of potential levels under illumination suggest that W-doping reduces charge carrier recombination in $BiVO_4$ films. LSVs shown in Figure 6a reveal significant enhancement in the PEC activity of W-doped $BiVO_4$ as compared to undoped. The highest photocurrents of ∼0.35 mA cm^{-2} at 1.4 V were obtained with W1_$BiVO_4$ and W5_$BiVO_4$ photoelectrodes, while higher doping resulted in poorer photoresponse. EIS measurements (Figure 6b) show that the pure $BiVO_4$ coating has an infinite charge transfer resistance (R_{ct}). However, after W-doping, R_{ct} values decreased to ∼1800 and ∼800 Ω for W10_$BiVO_4$ and W1_$BiVO_4$ and W5_$BiVO_4$ coatings, respectively. The equivalent circuit used to fit the EIS data is shown in the inset in Figure 6b. This model effectively describes the interfacial charge transfer and diffusion phenomena occurring in porous coatings. The circuit consists of the electrolyte solution resistance (R_s); the charge transfer resistance at the electrode/electrolyte interface (R_{ct}); the double-layer capacitance (C_{dl}), represented by a constant phase element (CPE) to account for non-ideal behavior; the resistance within the porous layer (R_s), related to ion migration in confined spaces and also represented by CPE; the capacitance associated with the porous layer (C_p); and the finite-length Warburg element, W_o, representing diffusion through the porous structure. The fitting results are summarized in Table 2.

Mott−Schottky measurements were conducted to evaluate the density of charge carriers in undoped and W-doped $BiVO_4$ films (Figure S4b,c). It can be observed that the curve for undoped $BiVO_4$ differs from those of W-modified coatings, where two linear regions can be seen. This is an indication of a complex charge distribution within the W-doped semiconductor material. The two linear regions might correspond to different electrical characteristics at different depths or regions of the layer. This could be related to a gradient of W-doping and an inhomogeneous charge distribution, resulting in different capacitance characteristics in different regions. The calculated charge carrier densities are shown in Table 2. For undoped $BiVO_4$, the N_D was 5.1×10^{18} while for W-doped $BiVO_4$, the value was up to an order of magnitude higher, confirming the effect of doping on donor density.

Although photoanodic current at $BiVO_4$ electrodes is often attributed to hole-induced oxidation of water molecules to oxygen, there is compelling evidence that the main products of photoanodic reactions in sulfate media are RSS, e.g., $S_2O_8^{2-}$.[10,40−42] In this study, W-doped $BiVO_4$ coatings were used in the photoelectrolysis of a 0.5 M Na_2SO_4 solution in a two-electrode cell with Pt cathode under applied bias of 1.2 V, and the products of both photoanodic and cathodic reactions were analyzed. The results of the chronoamperometric measurements summarized in Figure 6c show that the W1_$BiVO_4$ and W5_$BiVO_4$ coatings gave the highest photocurrents and the highest Faradaic efficiencies of almost 90% of the PEC generation of RSS. The W5_$BiVO_4$ sample outperformed the others in terms of its photocurrent stability. The performance of the W10_$BiVO_4$ coating was significantly inferior in terms of photocurrent density and FE of RSS production (43.8 ± 5%). In the case of pure $BiVO_4$, the amount of persulfate was below the detection limit of the titrimetric analysis applied in this work. FE values lower than 100% are most likely due to other competing reactions that occur on the surface of the photoanodes, e.g., oxidation of water molecules. Possible mechanisms of hole-induced formation of $S_2O_8^{2-}$ in aqueous sulfate electrolyte using WO_3 and WO_3/$BiVO_4$ photoanodes have been analyzed in

https://doi.org/10.1021/acsaem.5c00150
ACS Appl. Energy Mater. 2025, 8, 7919−7928

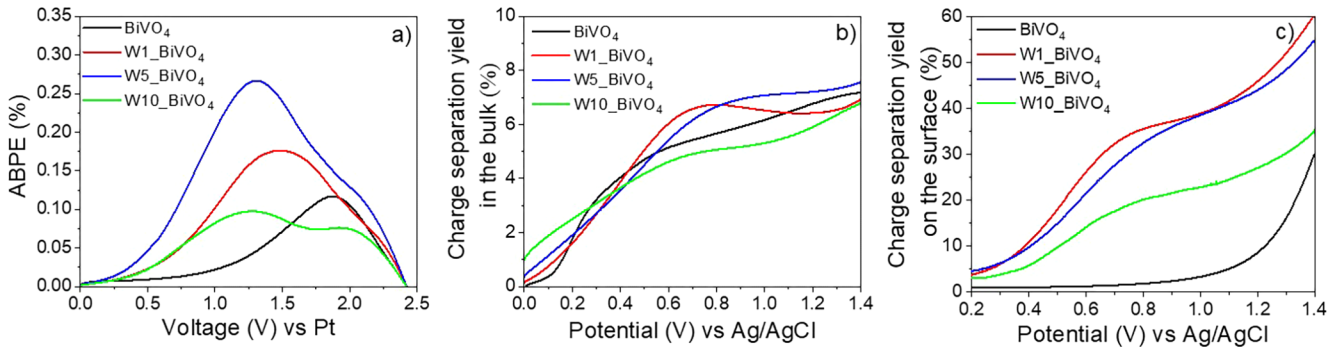

Figure 7. Results of ABPE (a), calculated charge separation yield in the bulk (b), and charge separation yield on the surface (c) for $BiVO_4$, W1_$BiVO_4$, W5_$BiVO_4$, and W10_$BiVO_4$ coatings.

detail in our recent study,[43] where radical-mediated ($HO^{\bullet}$, $SO_4^{\bullet -}$) and nonradical reaction pathways have been proposed. It is noteworthy that FE values of light-driven generation of persulfate ranging between 70 and 90% have been found for Mo-doped $BiVO_4$ as well.[10] Figure 6d shows the variation of hydrogen concentration in the photoelectrolysis cell, which was simultaneously monitored in the same experiment. The results are consistent with the magnitude of the photocurrent, i.e., the most rapid increase in H_2 concentration was observed for W1_$BiVO_4$ and W5_$BiVO_4$ samples, whereas the amount of H_2 produced by the W10_$BiVO_4$ and undoped $BiVO_4$ coatings was below the limit of detection, mostly due to low photocurrent. On the basis of these results, the main overall process occurring in the PEC cell can be written as follows:

$$2SO_4^{2-} + 2H_2O \rightarrow S_2O_8^{2-} + H_2 + 2OH^- \quad \text{(R1)}$$

The local increase in pH generated by reaction R1 should shift the hydrogen evolution reaction to more negative potentials, making this process self-limiting. This is most likely the reason why H_2 concentration in the case of W1_$BiVO_4$ and W5_$BiVO_4$ electrodes reaches saturation at longer electrolysis times (>4000 s) (Figure 6d).

Photocurrent stability tests were conducted under the same conditions as those used for the production of persulfate species and hydrogen evolution (Figure S6). Although W1_$BiVO_4$ outperformed the other samples during the first 2 h of the experiment, by the end of the nearly 8 h test, the photocurrents of all W-doped samples were virtually equal, highlighting the need to improve the stability of the material.

Next, the ABPE of the PEC generation of persulfate and hydrogen was evaluated (Figure 7a). The highest ABPE value of approximately 0.27% was found for the W5_$BiVO_4$ coating, while W1_$BiVO_4$ showed a value of about 0.15%. It is noteworthy that the ABPE plots of W-doped $BiVO_4$ show two peaks—a larger one within 1.2−1.7 V (vs Pt) and a smaller one at ∼2 V (vs Pt), similar to the IPCE plots shown in Figure 5. The position of the smaller peak coincides with that of the single peak of undoped $BiVO_4$. This is an additional indication that doping with W introduces a certain fraction of electronic states, the participation of which in photoinduced charge transfer reactions is more facile compared with undoped $BiVO_4$. These observations are consistent with the results of FLIM, IPCE, and Mott-Schottky measurements, which corroborate the inhomogeneity of W-doped $BiVO_4$ coatings (Figures 4 and 5 and Figure S4b, c).

In order to better understand the reasons for different performances of the W-doped and undoped $BiVO_4$ coatings, charge separation yields in the bulk (η_{bulk}) and on the surface (η_{surf}) of the photoelectrode were evaluated based on the method described in the Section 2. Interestingly, values of η_{bulk} were rather low, not exceeding 8% for all of the coatings, and no clear effect of W-doping was observed (Figure 7b). In the case of η_{surf}, however, the situation was completely different. W-doping led to a significant enhancement of charge carrier separation on the surface even at low values of applied bias. Optimal results were achieved with W1_$BiVO_4$ and W5_$BiVO_4$ coatings where η_{surf} increased rapidly with applied potential and reached 55−60% at 1.4 V. In the case of W10_$BiVO_4$, the increase in η_{surf} was slower, and the maximum attained value was ∼35%, whereas for undoped $BiVO_4$ η_{surf} stayed below 10% until the potential reached 1.2 V, indicating a significant degree of recombination at the surface.

The results obtained suggest that the mechanism of PEC performance enhancement in W-doped $BiVO_4$ is related to the reduction of charge recombination at the photoelectrode surface. The improved charge separation can be related to the ability of the dopant to change its oxidation state ($W^{6+} \rightleftharpoons W^{5+}$) depending on local conditions during the PEC process and thus act as an electron reservoir, which helps to trap and shuttle photoelectrons more efficiently. It seems probable that the defects introduced by W-doping are associated with the electronic states described above, which require lower energy input to excite and participate in the interfacial charge transfer. The presence of such states is manifested by additional peaks in the IPCE and ABPE plots, observed at higher wavelengths and/or lower applied-bias values, and by the presence of two linear regions in the Mott-Schottky plots. The easier extraction of these charge carriers is most likely related to the superficial position of the lattice defects introduced by the W-doping, leading to more efficient charge separation at the surface. Similar observations have been reported by Talasila et al.,[44] who showed that increasing the amount of W-doping results in higher carrier densities, but it also increases the distortion of the $BiVO_4$ structure, which, if the amount of dopant is too high (in their case 9 wt %), ultimately compromises the photoelectroactivity of the doped material. When the concentration of dopants is too high, they act as scattering centers that significantly impede charge transport.[31] Using the synthesis procedure adopted in this study, the optimal W-doping level was found to be between 1 and 5%, while increasing the dopant concentration to 10% had a detrimental effect.

https://doi.org/10.1021/acsaem.5c00150
ACS Appl. Energy Mater. 2025, 8, 7919−7928

4. CONCLUSIONS

The findings of the study demonstrate that the PEC performance of $BiVO_4$ coatings in aqueous sulfate electrolytes is significantly influenced by W-doping, which affects the formation of defects in the crystal lattice of the material. With the studied amount of W dopant ranging between 0 and 10 atom %, the optimal results in terms of PEC activity were achieved for the coatings doped with 1 and 5 atom % of W (W1_$BiVO_4$ and W5_$BiVO_4$). FLIM and SPV measurements revealed a more efficient charge carrier separation in the W1_$BiVO_4$ and W5_$BiVO_4$ materials. The analysis of charge separation yields showed that charge separation in the bulk was the limiting factor for the PEC performance of all the studied materials, whereas W-doping was found to reduce charge carrier recombination at the surface. The presence of two maxima in the IPCE and ABPE plots, along with two linear regions in the Mott–Schottky plots of W-doped $BiVO_4$, was attributed to chemical and structural inhomogeneity introduced by W-doping, which created regions with distinct electronic properties. It was suggested that enhanced charge separation at the surface results from the superficial position of $BiVO_4$ lattice defects introduced by W-doping.

The applicability of the coatings for the light-induced production of persulfate and hydrogen in an aqueous sulfate medium was demonstrated. The faradaic efficiency of $S_2O_8^{2-}$ formation in the case of W1_$BiVO_4$ and W5_$BiVO_4$ photoelectrodes ranged between 84 and 88% (±5%). These results are expected to be valuable for future research aimed at developing sustainable and innovative technologies that align with the objectives of the EU decarbonization plan.

■ ASSOCIATED CONTENT

Supporting Information

The Supporting Information is available free of charge at https://pubs.acs.org/doi/10.1021/acsaem.5c00150.

Figures and tables supporting the main text; characterization, PEC performance data, and stability tests (PDF)

■ AUTHOR INFORMATION

Corresponding Author

Arunas Ramanavicius − *Institute of Chemistry, Faculty of Chemistry and Geosciences, Department of Physical Chemistry, Vilnius University, Vilnius LT- 03225, Lithuania; Department of Nanotechnology, Centre for Physical Sciences and Technology, Vilnius LT-10257, Lithuania;* orcid.org/0000-0002-0885-3556; Email: Arunas.Ramanavicius@chf.vu.lt

Authors

Milda Petruleviciene − *Department of Chemical Engineering and Technology, Centre for Physical Sciences and Technology, Vilnius LT-10257, Lithuania;* orcid.org/0000-0003-0440-8815

Kaja Spilarewicz − *Faculty of Chemistry, Jagiellonian University, Kraków 30-387, Poland;* orcid.org/0000-0001-8428-8387

Irena Savickaja − *Department of Chemical Engineering and Technology, Centre for Physical Sciences and Technology, Vilnius LT-10257, Lithuania;* orcid.org/0000-0001-6918-7975

Jurga Juodkazyte − *Department of Chemical Engineering and Technology, Centre for Physical Sciences and Technology, Vilnius LT-10257, Lithuania;* orcid.org/0000-0003-1265-8320

Joanna Kuncewicz − *Faculty of Chemistry, Jagiellonian University, Kraków 30-387, Poland;* orcid.org/0000-0002-0414-6918

Grażyna Stochel − *Faculty of Chemistry, Jagiellonian University, Kraków 30-387, Poland;* orcid.org/0000-0002-9502-6371

Wojciech Macyk − *Faculty of Chemistry, Jagiellonian University, Kraków 30-387, Poland;* orcid.org/0000-0002-1317-6115

Complete contact information is available at: https://pubs.acs.org/10.1021/acsaem.5c00150

Author Contributions

Milda Petruleviciene: experimental analysis, writing (original draft), visualization, investigation. Irena Savickaja: experimental analysis. Jurga Juodkazyte: visualization, writing (review and editing). Kaja Spilarewicz: experimental analysis, investigation, visualization. Joanna Kuncewicz: experimental analysis, investigation, visualization. Grażyna Stochel: experimental analysis, investigation. Wojciech Macyk: supervision, writing (review and editing). Arunas Ramanavicius: supervision, writing (review and editing).

Notes

The authors declare no competing financial interest.

■ ACKNOWLEDGMENTS

This research was funded from postdoctoral fellowship project, No. S-PD-22-2, funded from Research Council of Lithuania (LMTLT). The study was carried out using research infrastructure funded by the European Union in the framework of the Smart Growth Operational Program, Measure 4.2; Grant No. POIR.04.02.00-00-D001/20, "ATOMIN 2.0—Center for Materials Research on ATOMic scale for the INnovative economy".

■ ABBREVIATIONS

ABPE Applied-bias photon-to-current efficiency; CA Chronoamperometry; DRS Diffuse reflectance spectroscopy; EDX Energy-dispersive X-ray; FLIM Fluorescence-lifetime imaging microscopy; GIXRD Grazing incidence X-ray diffraction; IPCE Incident photon-to-current efficiency; LSV Linear sweep voltammetry; OCP Open-circuit potential; PEC Photoelectrochemical; PEC AOS Photoelectrochemical advanced oxidation systems; SEM Scanning electron microscopy; SPV Surface photovoltage; XRD X-ray diffraction

■ REFERENCES

(1) Wang, Y.; Zhang, J.; Balogun, M. S.; Tong, Y.; Huang, Y. Oxygen Vacancy–based Metal Oxides Photoanodes in Photoelectrochemical Water Splitting. *Mater. Today Sustain.* **2022**, *18*, No. 100118.

(2) Hamdani, I. R.; Bhaskarwar, A. N. Recent Progress in Material Selection and Device Designs for Photoelectrochemical Water-Splitting. *Renew. Sustain. Energy Rev.* **2021**, *138*, No. 110503.

(3) Hassan, N. S.; Jalil, A. A.; Rajendran, S.; Khusnun, N. F.; Bahari, M. B.; Johari, A.; Kamaruddin, M. J.; Ismail, M. Recent Review and Evaluation of Green Hydrogen Production via Water Electrolysis for a Sustainable and Clean Energy Society. *Int. J. Hydrogen Energy* **2024**, *52*, 420–441.

(4) Orimolade, B. O.; Arotiba, O. A. Bismuth Vanadate in Photoelectrocatalytic Water Treatment Systems for the Degradation

of Organics: A Review on Recent Trends. *J. Electroanal. Chem.* **2020**, *878*, No. 114724.
(5) Hardwick, T.; Qurashi, A.; Shirinfar, B.; Ahmed, N. Interfacial Photoelectrochemical Catalysis: Solar-Induced Green Synthesis of Organic Molecules. *ChemSusChem* **2020**, *13* (8), 1967−1973.
(6) Galushchinskiy, A.; González-Gómez, R.; McCarthy, K.; Farràs, P.; Savateev, A. Progress in Development of Photocatalytic Processes for Synthesis of Fuels and Organic Compounds under Outdoor Solar Light. *Energy Fuels* **2022**, *36* (9), 4625−4639.
(7) Mousset, E.; Dionysiou, D. D. Photoelectrochemical Reactors for Treatment of Water and Wastewater: A Review. *Environ. Chem. Lett.* **2020**, *18* (4), 1301−1318.
(8) Petruleviciene, M.; Parvin, M.; Savickaja, I.; Gece, G.; Naujokaitis, A.; Pakstas, V.; Pilipavicius, J.; Gegeckas, A.; Gaigalas, G.; Juodkazyte, J. WO_3 Coatings for Photoelectrochemical Synthesis of Persulfate: Efficiency, Stability and Applicability. *J. Solid State Electrochem.* **2022**, *26* (4), 1021−1035.
(9) Juodkazytė, J.; Petrulevičienė, M.; Parvin, M.; Šebeka, B.; Savickaja, I.; Pakštas, V.; Naujokaitis, A.; Virkutis, J.; Gegeckas, A. Activity of Sol-Gel Derived Nanocrystalline WO_3 Films in Photoelectrochemical Generation of Reactive Chlorine Species. *J. Electroanal. Chem.* **2020**, *871*, No. 114277.
(10) Petruleviciene, M.; Savickaja, I.; Juodkazyte, J.; Grinciene, G.; Ramanavicius, A. Investigation of $BiVO_4$-Based Advanced Oxidation System for Decomposition of Organic Compounds and Production of Reactive Sulfate Species. *Sci. Total Environ.* **2023**, *875*, No. 162574.
(11) Petruleviciene, M.; Turuta, K.; Savickaja, I.; Juodkazyte, J.; Ramanavicius, A. Photoelectrochemical Degradation of Organic Compounds via Formed Reactive Chlorine and Sulfate Species by WO_3-Based Photoanodes. *J. Electroanal. Chem.* **2023**, *951*, No. 117954.
(12) Taga, Y.; Pan, Z.; Katayama, K.; Sohn, W. Y. BiVO4-Dotted WO_3 Photoanode with an Inverse Opal Underlayer for Photoelectrochemical Water Splitting. *ACS Appl. Energy Mater.* **2022**, *5*, 5750−5755.
(13) Swathi, S.; Babu, E. S.; Yuvakkumar, R.; Ravi, G.; Chinnathambi, A.; Alharbi, S. A.; Velauthapillai, D. Branched and Unbranched ZnO Nanorods Grown via Chemical Vapor Deposition for Photoelectrochemical Water-Splitting Applications. *Ceram. Int.* **2021**, *47* (7), 9785−9790.
(14) Venkata Reddy, C.; Reddy, I. N.; Akkinepally, B.; Reddy, K. R.; Shim, J. Synthesis and Photoelectrochemical Water Oxidation of (Y, Cu) Codoped α-Fe_2O_3 Nanostructure Photoanode. *J. Alloys Compd.* **2020**, *814*, No. 152349.
(15) Han, Y.; Wu, J.; Li, Y.; Gu, X.; He, T.; Zhao, Y.; Huang, H.; Liu, Y.; Kang, Z. Carbon Dots Enhance the Interface Electron Transfer and Photoelectrochemical Kinetics in TiO_2 Photoanode. *Appl. Catal. B Environ.* **2022**, *304*, No. 120983.
(16) Liu, K.; Zhou, H.; Wang, P.; Fang, J.; Li, H.; Cao, M.; Gao, X.; Qiu, X.; Liu, M. Bismuth Vanadate Single Crystal Particles Modified with Tungsten for Efficient Photoeletrochemical Water Oxidation. *Catal. Today* **2019**, *335*, 511−519.
(17) Kalanoor, B. S.; Seo, H.; Kalanur, S. S. Multiple Ion Doping in $BiVO_4$ as an Effective Strategy of Enhancing Photoelectrochemical Water Splitting: A Review. *Mater. Sci. Energy Technol.* **2021**, *4*, 317−328.
(18) Cheng, C.; Fang, Q.; Fernandez-Alberti, S.; Long, R. Controlling Charge Carrier Trapping and Recombination in $BiVO_4$ with the Oxygen Vacancy Oxidation State. *J. Phys. Chem. Lett.* **2021**, *12* (14), 3514−3521.
(19) Zachäus, C.; Abdi, F. F.; Peter, L. M.; Van De Krol, R. Photocurrent of $BiVO_4$ Is Limited by Surface Recombination, Not Surface Catalysis. *Chem. Sci.* **2017**, *8* (5), 3712−3719.
(20) Bhatt, M. D.; Lee, J. Y. Theoretical Insights into the Mechanism of Oxygen Evolution Reaction (OER) on Pristine $BiVO_4$(001) and $BiVO_4$(110) Surfaces in Acidic Medium Both in the Gas and Solution (Water) Phases. *Nanotechnology* **2021**, *32* (33), 335401.
(21) Tayebi, M.; Lee, B. K. The Effects of W/Mo-Co-Doped $BiVO_4$ Photoanodes for Improving Photoelectrochemical Water Splitting Performance. *Catal. Today* **2021**, *361*, 183−190.
(22) Pakeetood, P.; Reunchan, P.; Boonchun, A.; Limpijumnong, S.; Munprom, R.; Ahuja, R.; T-Thienprasert, J. Hybrid-Functional Study of Native Defects and W/Mo-Doped in Monoclinic-Bismuth Vanadate. *J. Phys. Chem. C* **2019**, *123* (23), 14508−14516.
(23) Shi, Q.; Murcia-López, S.; Tang, P.; Flox, C.; Morante, J. R.; Bian, Z.; Wang, H.; Andreu, T. Role of Tungsten Doping on the Surface States in $BiVO_4$ Photoanodes for Water Oxidation: Tuning the Electron Trapping Process. *ACS Catal.* **2018**, *8* (4), 3331−3342.
(24) Zhao, X.; Hu, J.; Chen, S.; Chen, Z. An Investigation on the Role of W Doping in $BiVO_4$ Photoanodes Used for Solar Water Splitting. *Phys. Chem. Chem. Phys.* **2018**, *20* (19), 13637−13645.
(25) Iguchi, S.; Miseki, Y.; Sayama, K. Efficient Hypochlorous Acid (HClO) Production: Via Photoelectrochemical Solar Energy Conversion Using a BiVO4 -Based Photoanode. *Sustain. Energy Fuels* **2018**, *2* (1), 155−162.
(26) Sayama, K. Production of High-Value-Added Chemicals on Oxide Semiconductor Photoanodes under Visible Light for Solar Chemical-Conversion Processes. *ACS Energy Lett.* **2018**, *3* (5), 1093−1101.
(27) Petruleviciene, M.; Savickaja, I.; Griguceviciene, A.; Naujokaitis, A.; Ramanauskas, R.; Juodkazyte, J. Optimization of $BiVO_4$ Coatings for High Yield Photoelectrochemical Production of Reactive Chlorine Species. *J. Photochem. Photobiol. A Chem.* **2023**, *443*, No. 114842.
(28) Pattengale, B.; Ludwig, J.; Huang, J. Atomic Insight into the W-Doping Effect on Carrier Dynamics and Photoelectrochemical Properties of BiVO4 Photoanodes. *J. Phys. Chem. C* **2016**, *120* (3), 1421−1427.
(29) Vignesh, R.; Mathy, V. P. B.; Geetha, G. V.; Sivakumar, R.; Sanjeeviraja, C. Temperature Induced Thermochromism of M-BiVO4 Thin Films Prepared by Sol-Gel Spin Coating Technique. *Mater. Lett.* **2021**, *285*, No. 129200.
(30) Kim, J. H.; Lee, J. S. Elaborately Modified $BiVO_4$ Photoanodes for Solar Water Splitting. *Adv. Mater.* **2019**, *31* (20), 1−35.
(31) Xiao, S.; Chen, H.; Yang, Z.; Long, X.; Wang, Z.; Zhu, Z.; Qu, Y.; Yang, S. Origin of the Different Photoelectrochemical Performance of Mesoporous $BiVO_4$ Photoanodes between the $BiVO_4$ and the FTO Side Illumination. *J. Phys. Chem. C* **2015**, *119* (41), 23350−23357.
(32) Zhao, L.; Wei, J.; Li, Y.; Han, C.; Pan, L.; Liu, Z. Photoelectrochemical Performance of W-Doped $BiVO_4$ Photoanode. *J. Mater. Sci. Mater. Electron.* **2019**, *30* (24), 21425−21434.
(33) Parmar, K. P. S.; Kang, H. J.; Bist, A.; Dua, P.; Jang, J. S.; Lee, J. S. Photocatalytic and Photoelectrochemical Water Oxidation over Metal-Doped Monoclinic $BiVO_4$ Photoanodes. *ChemSusChem* **2012**, *5* (10), 1926−1934.
(34) Liang, Y.; Tsubota, T.; Mooij, L. P. A.; Van De Krol, R. Highly Improved Quantum Efficiencies for Thin Film $BiVO_4$ Photoanodes. *J. Phys. Chem. C* **2011**, *115* (35), 17594−17598.
(35) Park, H. S.; Kweon, K. E.; Ye, H.; Paek, E.; Hwang, G. S.; Bard, A. J. Factors in the Metal Doping of $BiVO_4$ for Improved Photoelectrocatalytic Activity as Studied by Scanning Electrochemical Microscopy and First-Principles Density-Functional Calculation. *J. Phys. Chem. C* **2011**, *115* (36), 17870−17879.
(36) Jia, Y.; Wang, Z.; Ma, Y.; Liu, J.; Shi, W.; Lin, Y.; Hu, X.; Zhang, K. Boosting Interfacial Charge Migration of TiO_2 /$BiVO_4$ Photoanode by W Doping for Photoelectrochemical Water Splitting. *Electrochim. Acta* **2019**, *300*, 138−144.
(37) Li, M.; Zhao, L.; Guo, L. Preparation and Photoelectrochemical Study of $BiVO_4$ Thin Films Deposited by Ultrasonic Spray Pyrolysis. *Int. J. Hydrogen Energy* **2010**, *35* (13), 7127−7133.
(38) Yang, Y.; Zhao, Y.; Fan, W.; Shen, H.; Shi, W. A Simple Flame Strategy for Constructing W-Doped $BiVO_4$ Photoanodes with Enhanced Photoelectrochemical Water Splitting. *Int. J. Energy Res.* **2020**, *44* (13), 10821−10831.
(39) Won, J. Y.; Pan, Z.; Pihosh, Y.; Sohn, W. Y. Investigation of the Origin of the Enhanced Photoelectrochemical Performance of

https://doi.org/10.1021/acsaem.5c00150
ACS Appl. Energy Mater. 2025, 8, 7919−7928

Gradient W-Doped Bismuth Vanadate ($BiVO_4$) Photoanodes. *Int. J. Hydrogen Energy* **2024**, *54*, 1544−1551.
(40) Parvin, M.; Petrulevičienė, M.; Savickaja, I.; Šebeka, B.; Karpicz, R.; Griguceviciene, A.; Ramanauskas, R.; Juodkazytė, J. Influence of Morphology on Photoanodic Behaviour of WO_3 Films in Chloride and Sulphate Electrolytes. *Electrochim. Acta* **2022**, *403*, No. 139710.
(41) Zheng, L. L.; Tian, L.; Wang, D.; Chen, Y.; Tang, Q. Q.; Xing, Q. J.; Liu, X. Z.; Wu, D. S.; Zou, J. P. Facet Engineering of $BiVO_4$ Photocatalyst for the Synergetic Adsorption and Activation of Persulfate for Organic Pollutants Degradation. *Chem. Eng. J.* **2023**, *473*, No. 145507.
(42) Pan, T.; Tang, Y.; Liao, Y.; Chen, J.; Li, Y.; Wang, J.; Li, L.; Li, X. $BiVO_4$ Modifying with Cobalt-Phosphate Cluster Cocatalyst for Persulfate Assisted Photoelectrocatalytic Degradation of Tetracycline. *Mol. Catal.* **2023**, *549*, No. 113527.
(43) Petruleviciene, M.; Savickaja, I.; Kovger-Jarosevic, J.; Juodkazyte, J.; Padarauskas, A.; Griguceviciene, A.; Ramanavicius, A. Photoelectrochemical Degradation of Diclofenac, Tetracycline, and Amoxicillin in an Aqueous Sulfate Medium: Analysis of Reactive Species. *ACS Omega* **2025**, *10*, 8538−8550.
(44) Talasila, G.; Sachdev, S.; Srivastva, U.; Saxena, D.; Ramakumar, S. S. V. Modified Synthesis of $BiVO_4$ and Effect of Doping (Mo or W) on Its Photoelectrochemical Performance for Water Splitting. *Energy Reports* **2020**, *6*, 1963−1972.
(45) Geronimo, L.; Ferreira, C. G.; Gacha, V.; Raptis, D.; Martorell, J.; Ros, C. Understanding the Internal Conversion Efficiency of $BiVO_4/SnO_2$ Photoanodes for Solar Water Splitting: An Experimental and Computational Analysis. *ACS Appl. Energy Mater.* **2024**, *7* (5), 1792−1801.
(46) Abdi, F. F.; Firet, N.; vandeKrol, R. Efficient $BiVO_4$ Thin Film Photoanodes Modified with Cobalt Phosphate Catalyst and W-Doping. *ChemCatChem.* **2013**, *5* (2), 490−496.

https://doi.org/10.1021/acsaem.5c00150
ACS Appl. Energy Mater. 2025, 8, 7919−7928